Effect of chemical pressure on the charge density wave transition in rare-earth tritellurides $R\text{Te}_3$

N. Ru,[1] C. L. Condron,[2] G. Y. Margulis,[1] K. Y. Shin,[1] J. Laverock,[3] S. B. Dugdale,[3] M. F. Toney,[2] and I. R. Fisher[1]

[1]*Geballe Laboratory for Advanced Materials and Department of Applied Physics, Stanford University,
Stanford, California 94305, USA*

[2]*Stanford Synchrotron Radiation Laboratory, Stanford Linear Accelerator Center, Menlo Park, California 94025, USA*

[3]*H. H. Wills Physics Laboratory, University of Bristol, Tyndall Avenue, Bristol BS8 1TL, United Kingdom*

The charge density wave transition is investigated in the bilayer family of rare-earth tritelluride $R\text{Te}_3$ compounds ($R=$Sm, Gd, Tb, Dy, Ho, Er, and Tm) via high-resolution x-ray diffraction and electrical resistivity. The transition temperature increases monotonically with increasing lattice parameter from 244(3) K for TmTe$_3$ to 416(3) K for SmTe$_3$. The heaviest members of the series, $R=$Dy, Ho, Er, and Tm, are observed to have a second transition at a lower temperature, which marks the onset of an additional charge density wave with wave vector almost equal in magnitude to the first, but oriented in the perpendicular direction.

I. INTRODUCTION

Charge density waves (CDWs) are electronic instabilities found in low-dimensional materials with highly anisotropic electronic structures.[1] Since the CDW is predominantly driven by Fermi-surface (FS) nesting, it is especially sensitive to pressure-induced changes in the electronic structure. A well known example is NbSe$_2$, for which the CDW can be completely suppressed by an applied pressure of 35 kbar, favoring the competing superconducting phase.[2] Chemical pressure (the incorporation of larger or smaller ions to expand or contract the crystal lattice) can be used to mimic the effect of external pressure, providing a valuable tuning parameter for such materials. In this regard, rare-earth containing compounds are particularly valuable because the lattice parameter can be varied over a wide range in an almost continuous fashion while keeping the band filling essentially unchanged. The rare-earth tritelluride $R\text{Te}_3$ compounds form for almost the entire rare-earth series, with $R=$La-Nd, Sm, and Gd-Tm,[3–5] and provide a unique opportunity to follow the effect of chemical pressure on FS nesting and CDW formation.

The rare-earth tritellurides have a crystal structure that is layered and weakly orthorhombic (space group $Cmcm$),[4] consisting of double layers of nominally square-planar Te sheets, separated by corrugated $R\text{Te}$ slabs. In this space group, the long b axis is perpendicular to the Te planes. For most of the rare earths, the material has an incommensurate lattice modulation at room temperature, with a single in-plane wave vector of approximately $(2/7)\,c^*$ ($c^*=2\pi/c$).[5–9] For the heaviest rare earths, the same modulation has been observed slightly below room temperature.[10] The band structure has been calculated for the unmodulated structure, yielding a simple FS consisting of slightly warped inner and outer diamond sheets formed from p_x and p_z orbitals of Te atoms in the square-planar layers, both doubled due to the effects of bilayer splitting, with minimal b-axis dispersion.[11] The susceptibility $\chi(q)$ has a peak at a wave vector which is identical, to within experimental error, with the observed incommensurate lattice modulation.[12–14] Angle resolved photoemission spectroscopy (ARPES) has revealed that portions of the FS which are nested by this wave vector are indeed gapped, implying that the gain in one-electron energy contributes to the CDW formation.[15–18] There is a small but finite electronic contribution to the heat capacity, and the resistivity is observed to be metallic down to the lowest temperatures, confirming the presence of a small fraction of ungapped, reconstructed FS in the CDW state.[7,19,20]

ARPES measurements have shown that the maximum value of the CDW gap scales with the lattice parameter, with published values of $\sim$280 meV for SmTe$_3$ (Ref. [15]) and $\sim$400 meV for CeTe$_3$.[16] This trend has been confirmed by optical conductivity measurements, which also reveal that the remaining fraction of ungapped FS in the CDW state is larger for compounds with smaller lattice parameters.[21,22] However, to date the most prominent feature of this class of material, the CDW transition, has not been reported for this family of compounds. In this paper, we identify the CDW transition via high-resolution x-ray diffraction and resistivity measurements, and show that the transition temperature T_c varies by a remarkable amount, over 200 K, across the rare-earth series. In addition, we observe a second transition for the heaviest members of the series—$R=$Dy, Ho, Er, and Tm—and we show for ErTe$_3$ that this marks the onset of a second CDW with a wave vector $q_2\approx(1/3)a^*$ of similar magnitude and perpendicular to the first. The presence of this second transition is intimately linked to the effect of chemical pressure on the electronic structure.

II. EXPERIMENTAL METHODS

Single crystals of $R\text{Te}_3$ were grown by slow cooling a binary melt as described previously.[20] The electrical resistivity was measured up to 450 K for geometric bars cut and cleaved from the larger as-grown crystals, using an LR-700 ac resistance bridge operating at 16 Hz. Typical contact resistances of $1-3$ Ω were achieved using sputtered gold pads. In-plane measurements were made for arbitrary current directions in the ac plane, using a standard four point contact geometry. The b-axis resistivity was measured using a modified Montgomery geometry, with one current and one voltage contact on the top face of the platelike crystal, and the other

voltage and current contacts on the bottom face. The aspect ratio of the equivalent isotropic crystal[23,24] was typically 1:1 or slightly less, indicating that this technique may slightly underestimate the absolute value of the b-axis resistivity. Several measurements were made for each compound in the series.

High-resolution single crystal x-ray diffraction experiments were performed at the Stanford Synchrotron Radiation Laboratory (SSRL) on Beamlines 7-2 and 11-3. Data were collected in reflection geometry using x-ray energies of 9–13 keV. Either 1 or 2 mrad slits or a Ge(111) crystal analyzer was used to define the diffracted beam. The sample was mounted in an Anton-Paar furnace for heating above room temperature, and kept in a flow of helium gas to prevent oxidation. For measurements below room temperature, an ARS displex refrigerator was used, with the sample under vacuum. Uncertainties in absolute values of both the CDW wave vector and superlattice peak intensities were larger for experiments performed in the displex refrigerator. Experiments were performed on TbTe$_3$ and ErTe$_3$ as representative examples of compounds in the series with one and two transitions, respectively.

III. RESULTS

A. Resistivity

Representative resistivity data for GdTe$_3$ and TbTe$_3$ are shown in Figs. 1(a) and 1(b), respectively. Absolute values of the resistivity have been normalized to the average of several measurements of different samples. As has been previously observed for this family of compounds, the resistivity is strongly anisotropic.[19,20] For both compounds, a clear feature can be seen for both current orientations, with an onset at $T_c=377(3)$ and 336(3) K for GdTe$_3$ and TbTe$_3$, respectively. There is no hysteresis between warming and cooling cycles. As described in the next section, x-ray diffraction measurements show that this feature marks the CDW transition for TbTe$_3$. Excepting the loss of spin-disorder scattering at $T_N=5.6$ K for TbTe$_3$, no other features were observed in either the resistivity or its derivative, suggesting that there are no additional CDW phase transitions below T_c for either compound. The resistivity curves for SmTe$_3$ are similar, with $T_c=416(3)$ K. Data for the lightest members of the series, LaTe$_3$, CeTe$_3$, NdTe$_3$, and PrTe$_3$, are linear up to our maximum temperature, and these compounds are presumed to have CDW transition temperatures greater than 450 K.

The resistivity data for the heavier members of the series ($R=$Dy, Ho, Er, and Tm) are shown in Figs. 2(a)–2(d). These are qualitatively different from those of the lighter rare earths, showing two transitions at T_{c1} and T_{c2}. Again, data are shown for both heating and cooling cycles, as well as for in-plane and b-axis orientations. Looking at the b-axis data—for which the current direction is better defined—the feature at T_{c2} is largest for the heaviest member of the series, TmTe$_3$. This feature then decreases in both magnitude and temperature for the lighter rare earths, vanishing for compounds lighter than DyTe$_3$.[25] The derivative $d\rho/dT$ for DyTe$_3$ is shown in the inset of Fig. 2(a) to highlight the feature at T_{c2}. In the next section, we identify for ErTe$_3$ that
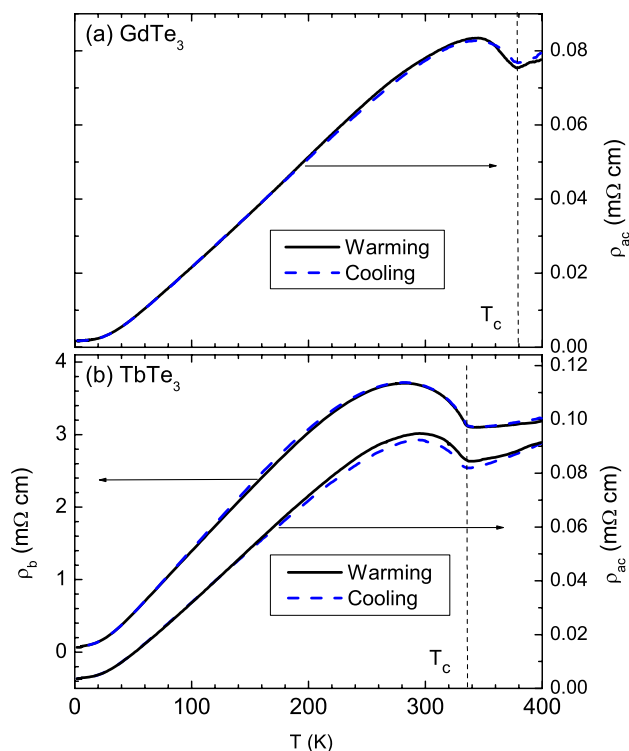

FIG. 1. (Color online) Temperature dependence of the resistivity of (a) GdTe$_3$ and (b) TbTe$_3$. Data are shown for currents oriented along the b axis (ρ_b, left axis) and arbitrary in-plane orientations (ρ_{ac}, right axis). Vertical axes are offset for clarity. Both warming (solid lines) and cooling (dashed lines) cycles are shown. T_c is marked by a vertical line.

T_{c2} marks the onset of a CDW with wave vector perpendicular to the first.

Figure 3 shows both CDW transition temperatures plotted as a function of the in-plane a-axis lattice parameter,[26] which provides a measure of the chemical pressure. The first transition temperature T_{c1} ranges from a low of 244(3) K for TmTe$_3$, the compound with the smallest lattice parameter in the series, and increases monotonically with increasing lattice parameter (decreasing chemical pressure). In contrast, the second transition temperature T_{c2} shows the opposite trend, *decreasing* as the lattice parameter increases, eventually vanishing halfway across the series.

B. X-ray diffraction of TbTe$_3$

X-ray diffraction data for TbTe$_3$ at room temperature reveal an incommensurate modulation wave vector $q=0.296(4)c^*$ and its harmonic $2q$. Here, for clarity, we reference the superlattice peak inside the first Brillouin zone, resulting in a wave vector $q\approx(2/7)c^*$, although ARPES[16] and scanning tunneling microscopy[9] (STM) results suggest that the equivalent $q'=c^*-q=0.704(4)c^*\sim(5/7)c^*$ has more physical meaning. Figure 4 shows representative diffraction patterns along the direction of the CDW wave vector for TbTe$_3$, as measured at SSRL Beamline 11-3 using 2 mrad slits. Intensities of Bragg peaks from the average
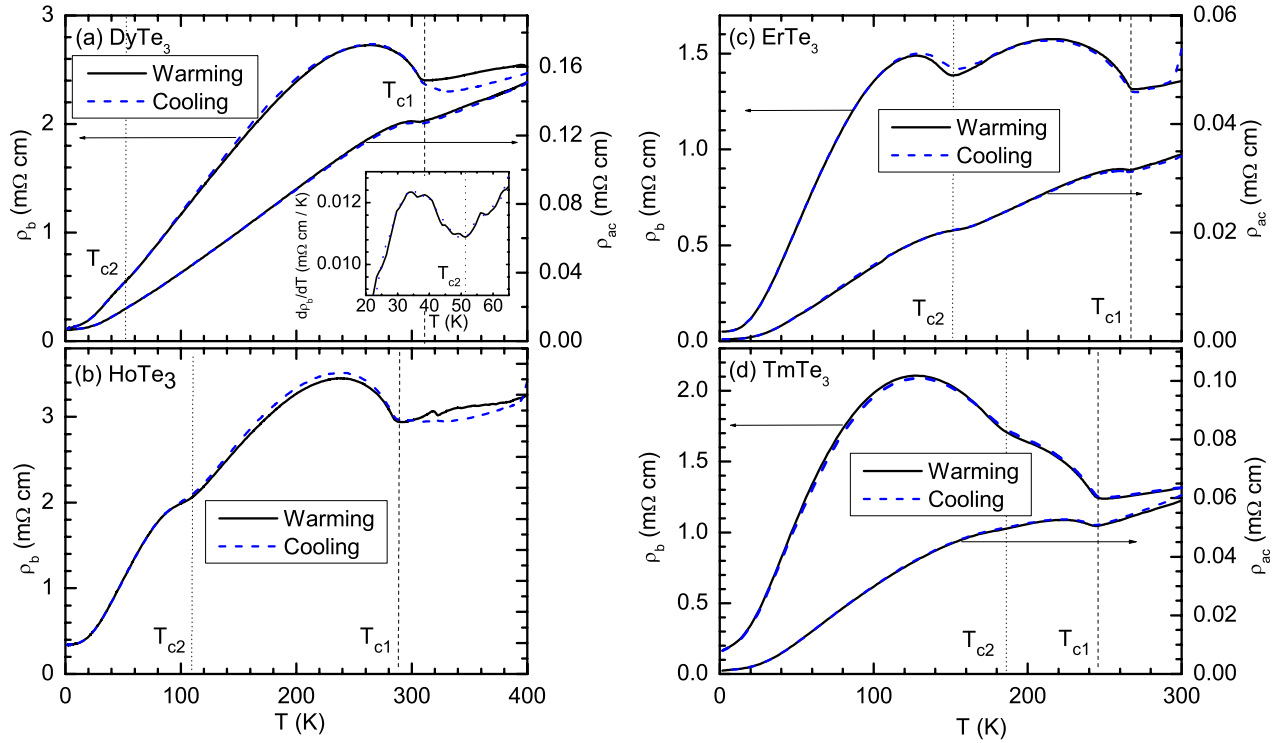
FIG. 2. (Color online) Temperature dependence of the resistivity of (a) DyTe$_3$ (inset: $d\rho/dT$), (b) HoTe$_3$, (c) ErTe$_3$, and (d) TmTe$_3$. Data are shown for current oriented along the b axis (ρ_b, left axis) and arbitrary in-plane orientations (ρ_{ac}, right axis). Both warming (solid lines) and cooling (dashed lines) cycles are shown. Both CDW transitions are marked for each compound.

crystal structure are indicated by open circles and are scaled down by a factor of 1000. First and second harmonic superlattice peaks are marked by blue and red arrows. Higher harmonics were not observed. The wave vector q and the equivalent q' are indicated on the lower panel. Both the

average structure Bragg peaks and the CDW superlattice peaks alternate in intensity, which can be attributed to the presence of two inequivalent Te atoms in the Te planes.[4]
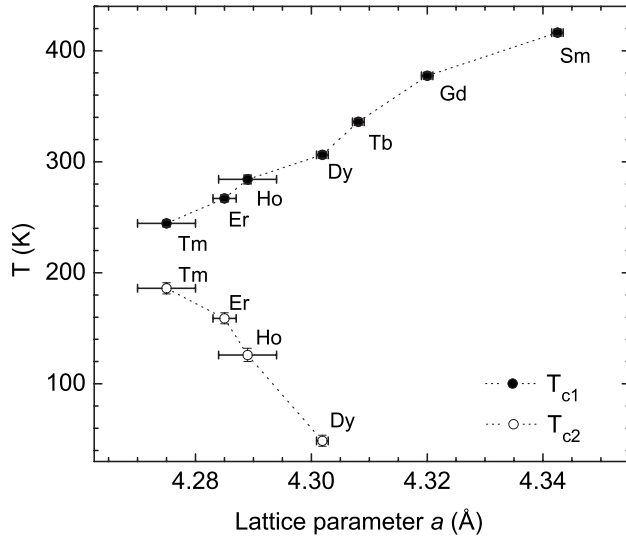

FIG. 3. T_{c1} and T_{c2}, as obtained from resistivity measurements, plotted as a function of in-plane lattice parameter a at 300 K (Ref. 26) for several compounds in the RTe$_3$ series (labeled). Note that the lattice parameter is smaller for the heavier members of the RTe$_3$ series. Dashed lines are drawn between points to guide the eye.
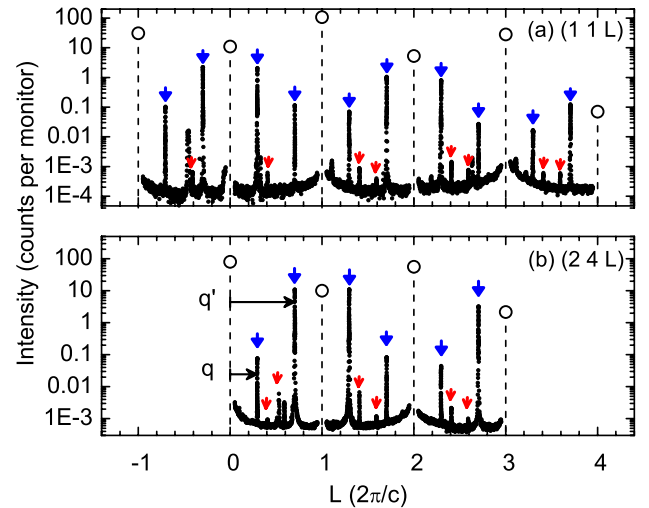

FIG. 4. (Color online) Representative x-ray diffraction patterns for TbTe$_3$ along (a) (1 1 L) and (b) (2 4 L) at room temperature. Intensities of Bragg peaks from the average structure are indicated by open circles and are scaled down by a factor of 1000. First and second harmonics of the CDW modulation are marked by blue and red arrows, respectively. The wave vector q and the alternate wave vector q' are marked.

The superstructure peaks in TbTe$_3$ are very sharp and, along with the average lattice peaks, were resolution limited in our experiments. The inset to Fig. 5(a) shows a typical superlattice peak as measured in high-resolution mode, using a Ge(111) crystal analyzer at SSRL Beamline 7-2. From this, we can draw lower bounds on the CDW correlation length ξ, calculated to be 1.8 μm within the Te planes and 0.5 μm perpendicular to the planes.

Heating measurements were taken with the sample mounted in an Anton-Paar furnace at SSRL Beamline 7-2 using a Ge(111) crystal analyzer. The integrated intensity of the (1 1 q) peak in TbTe$_3$ was followed as a function of temperature. Figure 5(a) shows the integrated intensity through the CDW transition for increasing and decreasing temperatures. The intensity rapidly decreases on heating from room temperature with no observable hysteresis, indicative of a second-order CDW transition as described theoretically.[12] Some scattering intensity, attributed to fluctuations, was observed above T_c up to 363 K, beyond which the peaks were too weak to distinguish from the background. Error bars shown are obtained from Lorentz fits to the individual scans. The full width at half maximum [FWHM, Fig. 5(b)] is resolution limited at lower temperatures and increases sharply at the CDW transition. The FWHM, being inversely proportional to the correlation length ξ, is fitted in the interval from 334 to 353 K to the expression $\xi^{-1} \approx (T - T_c)^\gamma$, where γ is taken as $2/3$ to correspond to the X-Y model universality class (complex order parameter and three dimensions). From this, we obtain a transition temperature $T_c = 332.8(5)$ K, which is drawn as a dotted vertical line through all four panels of Fig. 5. Within error, this value of T_c corresponds to that obtained from resistivity measurements [336(3) K].

The CDW transition in TbTe$_3$ is also reflected in the temperature dependence of the in-plane lattice parameters a and c [Fig. 5(c)]. Above T_c, a and c have a similar dependence, increasing linearly with temperature, and with a small relative difference of only 0.031% at 370 K. Formation of the CDW appears to "stretch" the lattice from its expected value along the direction of the modulation wave vector (c axis), while slightly compressing the lattice in the perpendicular direction, such that the relative difference between a and c at 300 K, 0.13%, is larger than above the CDW transition.

The absolute value of the CDW wave vector for TbTe$_3$ is plotted in Fig. 5(d). The absolute value of q does not vary significantly with temperature between room temperature and T_c. For temperatures above T_c, the absolute value of q decreases with increasing temperature.

Measurements for TbTe$_3$ were extended from room temperature down to 25 K by using an ARS displex refrigerator at SSRL Beamline 7-2 using 1 mrad slits. Figure 6(a) shows the temperature dependence of the square root of the integrated intensity, which is proportional to the order parameter,[1] together with the standard BCS curve. Data have been normalized by taking the average of the first four data points, from 30 to 100 K, and setting this value to unity. The close correspondence between the data and the BCS result confirms that the system can be treated within the weak-coupling limit. Error bars shown are ±20% of the integrated intensity, and represent the scatter associated with difficulties
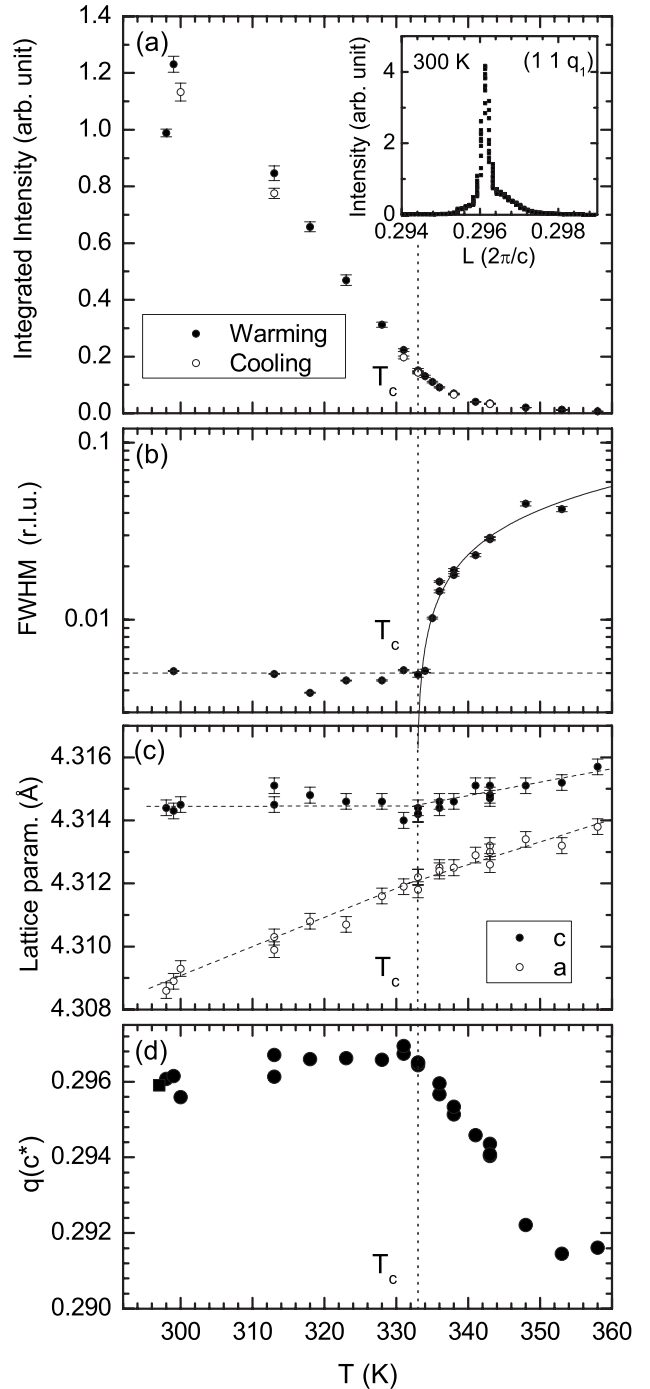

FIG. 5. (a) Temperature dependence of the integrated intensity of the (1 1 q) superlattice peak of TbTe$_3$ through T_c for increasing and decreasing temperatures. Inset: Raw data showing L scan for (1 1 q) at room temperature. (b) FWHM in the out-of-plane direction for the (1 7 q) superlattice peak. A dashed horizontal line marks the limit of resolution. The solid curve is $\xi^{-1} \sim (T - T_c)^\gamma$ with $T_c = 332.8(5)$ K and $\gamma = 2/3$. (c) The in-plane lattice parameters a and c, with lines drawn to guide the eye. (d) The absolute value of q as a function of temperature. T_c is indicated by a dashed vertical line in all four panels.
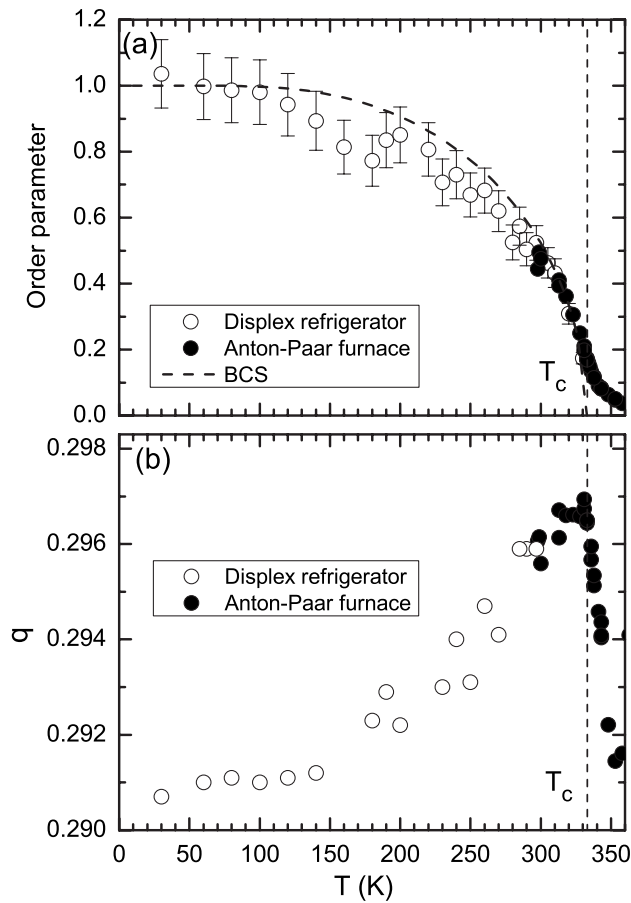
FIG. 6. (a) Temperature dependence of the square root of the integrated intensity of the $(1\ 1\ q)$ superlattice peak of TbTe$_3$, which is proportional to the order parameter. Data are normalized to unity at $T=0$. (b) The absolute value of q over the same temperature range. T_c is indicated by a dashed vertical line in both panels.

of centering the sample within the refrigerator. The apparent dip in the experimental data at approximately 150 K does not correlate with any additional features in the resistivity, and is most likely an experimental artifact.

Finally, the wave vector q [Fig. 6(b)] remains incommensurate to the lowest temperatures, and does not exhibit a lock-in transition.

C. X-ray diffraction of ErTe$_3$

To explore the case with two transitions, single crystal x-ray diffraction experiments were performed for ErTe$_3$ with the sample mounted in an ARS displex refrigerator at SSRL Beamline 7-2. An incommensurate modulation similar to TbTe$_3$ with $q_1 \approx (2/7)c^*$ was found in the temperature region $T_{c2} < T < T_{c1}$, as also noted by Malliakas and Kanatzidis.[10] For temperatures $T < T_{c2}$, an additional ordering along a^* was observed, perpendicular to the first wave vector. As investigated at 10 K using a Ge(111) crystal analyzer, the wave vector of this additional ordering was $q_2=0.343(5)a^*$, whereas that of the original ordering was $q_1=0.300(5)c^*$. Again, these values are cited in the first Brillouin zone

even though the equivalent values $q_1'=c^*-q_1=0.700(5)c^*$ and $q_2'=a^*-q_2=0.657(5)a^*$ may have more physical meaning for this system.[9,16] The absolute value of q_2 is close but not identical to that of q_1.

A section of reciprocal space explored at 10 K is shown in Fig. 7(a). Here, $K=3$ (remember that b is the long axis), $L \in [3.5\ 5.5]$, and $H \in [0.5\ 3.5]$. Filled symbols are those that were investigated, and open symbols are those assumed to be present from symmetry. Bragg peaks for the average structure are marked by large (black) circles. Note that for $K > 0$, these are extinct for $H+K=$odd. The superlattice peaks $q_1 \approx (2/7)c^*$ are shown as (red) upward-pointing triangles, with second harmonics in smaller (pink) upward-pointing triangles. The superlattice peaks $q_2 \approx (1/3)a^*$ are shown as (blue) triangles pointing to the right, with smaller (cyan) triangles denoting the second harmonics. Superlattice peaks at the linear combination q_1+q_2, denoted as (purple) stars, were also observed, providing further evidence that these two wave vectors are real and present in the same crystallite.

Raw data taken at 155 K using a Ge(111) crystal analyzer are shown in Figs. 7(b) and 7(c) for superlattice peaks q_1 and q_2, respectively. At this temperature, $q_1=0.298(5)c^*$ and $q_2 =0.344(5)a^*$. The FWHM for these peaks is larger for ErTe$_3$ due to a larger crystal mosaic, yet it remains clear that the magnitudes of q_1 and q_2 are very close but not identical.

Temperature dependent measurements were performed on selected superlattice peaks in ErTe$_3$. The integrated intensities of a q_1 peak $(-1\ 3\ 2+q_1)$ and a second harmonic of q_1 $(-1\ 3\ 3-2q_1)$ were measured using 1 mrad slits. Integrated intensities were normalized to the main Bragg peak $(-1\ 3\ 2)$. In Fig. 7(d), as for TbTe$_3$, the square root of the integrated intensity of the first harmonic is plotted with the average of the first four data points (from 25 to 100 K) normalized to 1. This agrees well with the BCS order parameter, which is plotted using a transition temperature of $T_{c1} =267(3)$ K as obtained from resistivity, and is shown as a dashed curve. The second harmonic superlattice peak can be considered as either a second-order diffraction harmonic of the first-order superlattice peak, or as the $2q_1$ component of a nonsinusoidal modulation.[27] In the first case, the integrated intensity of the second harmonic would be proportional to the order parameter to the fourth power.[28] In Fig. 7(d), the fourth root of the integrated intensity of $(-1\ 3\ 3-2q_1)$, with the average of the first four data points normalized to 1, is shown to agree with the BCS curve. This is consistent with the case of the purely sinusoidal modulation, although the presence of nonsinusoidal components cannot be ruled out. Just above T_{c2}, there is a small dip in intensities of both peaks. Although this could be a sign of the second CDW interacting with the first, errors are such that this dip should not be overly interpreted. Error bars shown are $\pm 10\%$ of the integrated intensity for both peaks.

Using a Ge(111) crystal analyzer, the temperature dependence of the q_2 peak $(1-q_2\ 6\ 4)$ was followed from 10 to 180 K. Shown in Fig. 7(e) is the integrated intensity from 140 to 180 K. The vertical dashed line is $T_{c2} =159(5)$ K as obtained from resistivity measurements. The integrated intensity decreases rapidly with increasing temperature across T_{c2}, similar to the behavior of q_1 through T_{c1}.
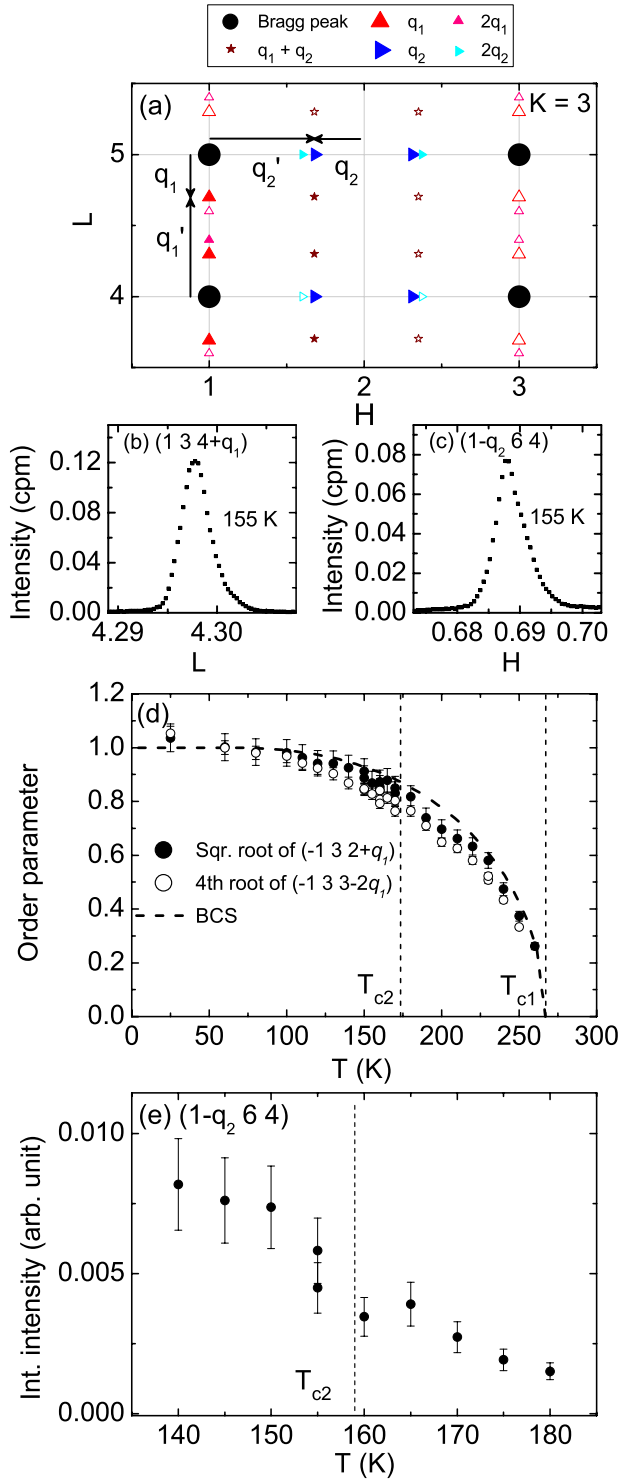
Error bars shown are ±20%. As in the case for TbTe$_3$ [Fig. 5(a)], scattering intensity is observed for several tens of kelvin above T_{c2}, indicative of the presence of substantial fluctuations.

IV. DISCUSSION

Here, we address the magnitude of T_{c1} for these materials, the origin of the second transition for the heaviest members of the rare-earth series, and the variation in T_{c1} and T_{c2} with chemical pressure.

First, we comment on the absolute value of T_{c1}. Taking TbTe$_3$ as an example, if the maximum value of the CDW gap as measured by ARPES [$\Delta \sim 240$ meV (Ref. 29)] is used to estimate a mean-field transition temperature via the familiar BCS expression, one obtains $T_{MF}(\max) \sim 1600$ K, over four times greater than the observed T_c of 336 K. However, since the FS of RTe$_3$ is not perfectly nested, the mean-field transition temperature will be substantially reduced from this value.[30–32] Furthermore, the observation of superlattice peaks with rapidly increasing FWHM and decreasing correlation length well above T_{c1} shows the presence of substantial fluctuations. These further reduce the critical temperature from the mean-field value, as has been previously observed for similar low-dimensional materials.[1]

To gain insight into the variation in the observed CDW transition temperatures, band structure calculations were performed for the unmodulated crystal structure for several members of the rare-earth series, using the linear muffin-tin orbital (LMTO) method within the atomic sphere approximation, including combined-correction terms.[33] The 4f electrons of the rare-earth elements were treated as open-core states. As input parameters for these calculations, we have used lattice parameters measured at 300 K taken from Ref. 10. For compounds for which 300 K is above the CDW transition, we have used the refined atomic positions in the *Cmcm* space group as published by Malliakas and Kanatzidis.[10] For compounds for which 300 K is below T_c, we have used the unmodulated *Cmcm* space group, but have taken the internal parameter (which defines the y position of the Te planes in the unit cell) from atomic refinements to the four-dimensional $C2cm(00\gamma)000$ space group[10] at 300 K.

Typical results illustrating the FS seen in projection down the b^* axis are shown in Fig. 8 for two specific compounds close to the ends of the rare-earth series, CeTe$_3$ and ErTe$_3$. The calculated Fermi surfaces for these two isoelectronic compounds are, as anticipated, broadly similar, with only subtle differences in topology at the very corners of the diamondlike sheets of FS. Both the bilayer splitting and the dispersion along the b^* axis (i.e., the thickness of the lines in Fig. 8) evolve weakly from CeTe$_3$ to ErTe$_3$, by $\sim +4\%$ in the first case, as measured by the separation of the two inner diamond sheets at $k_x = 0.16a^*$, and by $\sim +12\%$ in the latter, also measured at the inner diamond sheets at $k_x = 0.16a^*$. The overall bandwidth increases from CeTe$_3$ to ErTe$_3$, and the density of states at E_F, $n(E_F)$, decreases almost linearly from 21.1 for CeTe$_3$ to 19.9 states/Ry per cell for ErTe$_3$, a variation of approximately 5% (Fig. 9).

Quantitative calculations of the critical temperature are difficult for an imperfectly nested system, but it is clear that
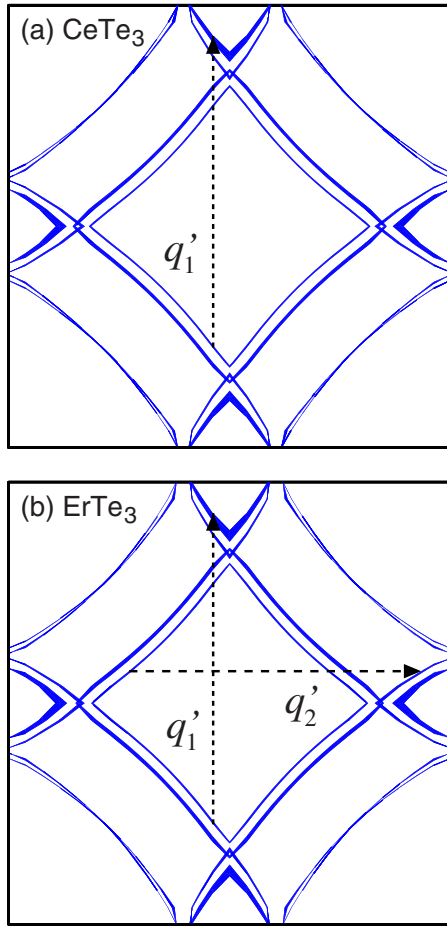
FIG. 7. (Color online) X-ray diffraction of ErTe$_3$. (a) Reciprocal lattice map. Solid symbols mark diffraction peaks found at 10 K. Hollow symbols mark peaks assumed to be present from symmetry. (b) L scan for $(1\ 3\ 4+q_1)$ at 155 K. (c) H scan for $(1-q_2\ 6\ 4)$ at 155 K. (d) The BCS order parameter (dashed line), plotted with the square root of the integrated intensity of $(-1\ 3\ 2+q_1)$, and the fourth root of the integrated intensity of $(-1\ 3\ 3-2q_1)$, both of which are normalized to unity at $T=0$. (e) Temperature dependence of the integrated intensity of $(1-q_2\ 6\ 4)$.

FIG. 8. (Color online) Fermi surface of (a) $CeTe_3$ and (b) $ErTe_3$ obtained from LMTO band structure calculations. The Fermi surface is shown in projection down the b^* axis such that the thickness of the lines is indicative of the b^*-axis dispersion of each of the bands. The horizontal dimension is k_x in the interval $\pm a^*/2$. The vertical dimension is k_z in the interval $\pm c^*/2$. The wave vectors q_1' and q_2' and corresponding nesting conditions are marked.
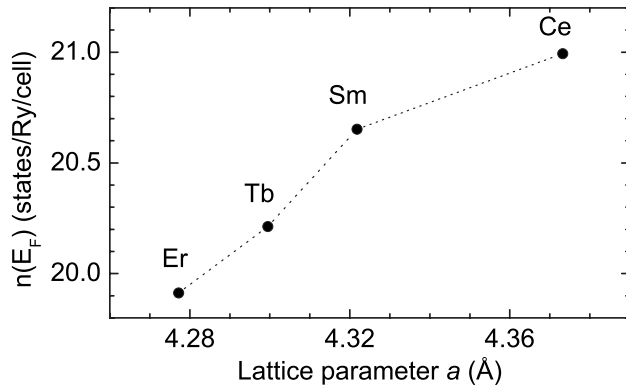

FIG. 9. Density of states at E_F for representative members of the RTe$_3$ series, as obtained from LMTO band structure calculations, shown as a function of the in-plane lattice parameter a. Dashed lines are drawn between the points to guide the eye.

all three effects described above will contribute to the decrease in T_{c1} with decreasing lattice parameter. The subtle variation in the b^*-axis dispersion and the bilayer splitting result in poorer nesting conditions, while the reduction in $n(E_F)$ directly affects the mean-field transition temperature. In the absence of more detailed calculations, we cannot determine the exact extent to which each of these effects contributes to the variation in T_{c1} across the rare-earth series. However, given that the mean-field transition temperature varies exponentially with $n(E_F)$, it is likely that the variation in $n(E_F)$ plays the dominant role.

The second CDW transition, observed only for the heaviest members of the rare-earth series, is particularly intriguing. Specifically, in contrast to most usual CDW transitions, the effect of increasing (chemical) pressure is actually to *increase* T_{c2}. It appears that this unusual behavior is directly linked to the variation in T_{c1}. In particular, the extent to which the FS is gapped below T_{c1} depends on the maximum size of the CDW gap. A reduction in the maximum gap causes a reduction in the total area of the FS that is gapped precisely because the FS is imperfectly nested. This is borne out by recent ARPES experiments, which reveal that for the compounds with smaller lattice parameters, the CDW gap extends a smaller distance around the FS from the tips of the diamond sheets at $k_x=0$.[18,29] Hence, on traversing the rare-earth series from LaTe$_3$ toward TmTe$_3$, progressively more of the FS remains intact below T_{c1}, and, as a consequence, is available for a subsequent CDW transition at a lower temperature. Having already lost the "tips" of the diamond sections of the FS that point in the c-axis direction at the first transition,[18] the second transition must involve sections of the FS closer to the tips of the diamonds pointing in the transverse a-axis direction. Indeed, these are exactly the regions of the FS that contribute to the competing peak in $\chi(q)$ found at $(2/7)a^*$ in band structure calculations for the unmodulated structure.[14] Preliminary ARPES results for ErTe$_3$ confirm this picture, revealing additional gaps forming on sections of the FS close to the tips of the diamond sections of the FS pointing in the a^* direction.[34] The corresponding jump in the resistivity at T_{c2}, related to the amount of FS gapped at the transition, is largest for the compound with the largest value of T_{c2} (smallest value of T_{c1}) and smallest area of initial FS gapped at T_{c1}. The resulting "rectangular" CDW state is characterized by orthogonal, independent wave vectors, almost equal in magnitude, but with an order parameter that is developed to a different degree in the two directions.

Yao *et al.* have recently addressed the question of the origin of the unidirectional CDW for the lightest members of the RTe$_3$ series.[12] Using a simple tight-binding model for a square lattice, and considering only noninteracting Te p_x and p_z bands, they found that for sufficiently high values of the electron-phonon coupling (and, consequently, T_c), a unidirectional ("stripe") CDW at 45° to the Te–Te bonds is favored over a bidirectional ("checkerboard") state in which p_x and p_z sheets of the FS are individually gapped by orthogonal wave vectors which are oriented at a different angle to the stripe phase. In this model, the stripe phase gaps a sufficient amount of the FS that only one of the two equivalent directions (a and c in the real material) is chosen for the lattice

modulation. The weak orthorhombicity of RTe$_3$ provides a natural symmetry breaking between the a and c axes such that for the lightest members of the series the unidirectional CDW is always observed along the c axis and never along a.[14] It will be intriguing to see whether this insightful toy model can be extended to incorporate the observed rectangular CDW phase at a more quantitative level than the qualitative arguments presented above.

Implicit in all of the above discussion has been the assumption that the electron-phonon coupling itself does not have a strong q dependence and does not vary substantially across the rare-earth series, though it is not necessarily immediately obvious that this should be the case. The Te–Te bond length in RTe$_3$ is substantially longer than the standard covalent bond length, implying that the unmodulated high-temperature structure of RTe$_3$ is inherently unstable, regardless of the low-dimensional electronic structure.[6] The close correspondence between the maxima in $\chi(q)$ and the observed superlattice wave vectors clearly demonstrates that the electronic system plays a preeminent role in the lattice modulation in this material. However, it is not clear whether it is the *only* driving force for the instability. To determine the relative role played by the lattice will take a substantial computational effort. However, this material appears to be a model system to quantitatively calculate the role played by an incipient lattice instability in CDW formation, something which to date has been lacking for most other CDW systems.[13]

V. CONCLUSIONS

The RTe$_3$ family of compounds has a remarkable phase diagram. All members of the series exhibit a CDW transition to a state characterized by a simple unidirectional incommensurate lattice modulation with wave vector $q_1 \approx (2/7)c^*$. The transition temperature T_{c1} is very sensitive to chemical pressure, varying by over 200 K across the series, principally ascribed to the variation in the density of states at the Fermi level $n(E_F)$. The heaviest members of the series exhibit an additional CDW transition at a lower temperature T_{c2}, with an almost equivalent wave vector oriented perpendicular to the first, along the a^* axis. The resulting rectangular CDW state consists of perpendicular modulation wave vectors almost equal in magnitude, but with independent order parameters, each developed to a different degree at any given temperature. These observations can be understood in terms of the second CDW nesting regions of the original FS that are ungapped by the first CDW. Specifically, on traversing the rare-earth series, as T_{c1} decreases, increasingly more of the remaining FS becomes available to drive a second CDW with a modulation wave vector transverse to the first.

We conclude by pointing out that by preparing samples with a continuous solid solution between adjacent rare earths in the lanthanide series, it would be possible to continuously tune the lattice parameter from that of LaTe$_3$ to that of TmTe$_3$ while retaining the same band filling. This exquisite degree of control of a physical parameter directly affecting the transition temperature, in conjunction with the remarkable simplicity of the stripe and rectangular CDW states, marks the rare-earth tritellurides as a model system for studying the effects of imperfect FS nesting on CDW formation.

[1] G. Gruner, *Density Waves in Solids* (Perseus, Cambridge, MA, 1994).

[2] C. Berthier, P. Molinie, and D. Jerome, Solid State Commun. **18**, 1393 (1976).

[3] E. Bucher, K. Andres, F. J. D. Salvo, J. P. Maita, A. C. Gossard, A. S. Cooper, and G. W. Hull, Phys. Rev. B **11**, 500 (1975).

[4] B. K. Norling and H. Steinfink, Inorg. Chem. **5**, 1488 (1966).

[5] E. DiMasi, M. C. Aronson, J. F. Mansfield, B. Foran, and S. Lee, Phys. Rev. B **52**, 14516 (1995).

[6] C. Malliakas, S. J. L. Billinge, H. J. Kim, and M. G. Kanatzidis, J. Am. Chem. Soc. **127**, 6510 (2005).

[7] Y. Iyeiri, T. Okumura, C. Michioka, and K. Suzuki, Phys. Rev. B **67**, 144417 (2003).

[8] H. J. Kim, C. D. Malliakas, A. T. Tomic, S. H. Tessmer, M. G. Kanatzidis, and S. J. L. Billinge, Phys. Rev. Lett. **96**, 226401 (2006).

[9] A. Fang, N. Ru, I. R. Fisher, and A. Kapitulnik, Phys. Rev. Lett. **99**, 046401 (2007).

[10] C. D. Malliakas and M. G. Kanatzidis, J. Am. Chem. Soc. **128**, 12612 (2006).

[11] J. Laverock, S. B. Dugdale, Z. Major, M. A. Alam, N. Ru, I. R. Fisher, G. Santi, and E. Bruno, Phys. Rev. B **71**, 085114 (2005).

[12] H. Yao, J. A. Robertson, E. A. Kim, and S. A. Kivelson, Phys. Rev. B **74**, 245126 (2006).

[13] I. Mazin and M. Johannes, arXiv:0708.1744 (unpublished).

[14] LMTO band structure calculations reveal almost equivalent peaks in $\chi(q)$ at $\approx (2/7)c^*$ and $\approx (2/7)a^*$, corresponding to nesting wave vectors between the inner and outer diamond sheets of the FS along the c^* and a^* directions, respectively. The peak at $(2/7)c^*$ is slightly larger in magnitude, and hence, determines the initial CDW wave vector if we assume a constant electron-phonon coupling. However, the difference is slight and is only apparent in these calculations when spin-orbit coupling is included [M. Johannes and I. Mazin (private communication)].

[15] G. H. Gweon, J. D. Denlinger, J. A. Clack, J. W. Allen, C. G. Olson, E. D. DiMasi, M. C. Aronson, B. Foran, and S. Lee, Phys. Rev. Lett. **81**, 886 (1998).

[16] V. Brouet, W. L. Yang, X. J. Zhou, Z. Hussain, N. Ru, K. Y. Shin, I. R. Fisher, and Z. X. Shen, Phys. Rev. Lett. **93**, 126405 (2004).

[17] H. Komoda, T. Sato, S. Souma, T. Takahashi, Y. Ito, and K. Suzuki, Phys. Rev. B **70**, 195101 (2004).

[18] ARPES measurements for $CeTe_3$ reveal a maximum gap of 400 meV at the Fermi energy for $k_x=0$ (i.e., the tips of the diamond sheets of the FS that are pointing along the c^* direction, see Fig. 8). The gap diminishes in magnitude the further one goes around the FS from this point, reaching zero at approximately $k_x=0.5a^*$ (Ref. 16). In comparison, for $SmTe_3$, for which the maximum gap is only 280 meV, the gap extends only as far as $k_x=0.35a^*$ (Ref. 29).

[19] E. DiMasi, B. Foran, M. C. Aronson, and S. Lee, Chem. Mater. **6**, 1867 (1994).

[20] N. Ru and I. R. Fisher, Phys. Rev. B **73**, 033101 (2006).

[21] A. Sacchetti, L. Degiorgi, T. Giamarchi, N. Ru, and I. R. Fisher, Phys. Rev. B **74**, 125115 (2006).

[22] A. Sacchetti, E. Arcangeletti, A. Perucchi, L. Baldassarre, P. Postorino, S. Lupi, N. Ru, I. R. Fisher, and L. Degiorgi, Phys. Rev. Lett. **98**, 026401 (2007).

[23] H. C. Montgomery, J. Appl. Phys. **42**, 2971 (1971).

[24] B. F. Logan, S. O. Rice, and R. F. Wick, J. Appl. Phys. **42**, 2975 (1971).

[25] While a second lower transition was not observed in the resistivity for $TbTe_3$, STM measurements on $TbTe_3$ at 6 K (Ref. 9) show an ordering with wave vector $\sim(2/3)a^*$, which is similar to q_2' as observed by x-ray diffraction in $ErTe_3$ below T_{c2}. This could mark the appearance of an extraordinary transition present only on the surface, or it could indicate that $TbTe_3$ does, in fact, have a second transition with $T_{c2}>6$ K, but with an accompanying resistivity feature too small to be observed.

[26] The lattice parameters for $GdTe_3$, $TbTe_3$, and $DyTe_3$ were obtained at SSRL BL11-3 by x-ray diffraction on single crystals. Lattice parameters for $SmTe_3$ from DiMasi *et al.* (Ref. 19). Lattice parameters for $HoTe_3$, $ErTe_3$, $TmTe_3$ from International Centre for Diffraction Data (ICDD) Powder Diffraction File (PDF) 2005.

[27] J. Pouget, C. Noguera, A. Moudden, and R. Moret, J. Phys. (Paris) **46**, 1731 (1985).

[28] A. J. C. Wilson, *X-ray Optics: The Diffraction of X-rays by Finite and Imperfect Crystals*, 2nd ed., Methuen's Monographs on Physical Subjects (Methuen, London, 1962).

[29] V. Brouet, W. L. Yang, X. J. Zhou, Z. Hussain, Z. X. Shen, J. Laverock, S. Dugdale, N. Ru, and I. R. Fisher (unpublished).

[30] K. Yamaji, J. Phys. Soc. Jpn. **51**, 2787 (1982).

[31] K. Yamaji, J. Phys. Soc. Jpn. **52**, 1361 (1983).

[32] K. Maki and A. Virosztek, J. Magn. Magn. Mater. **90/91**, 758 (1990).

[33] B. Barbiellini, S. B. Dugdale, and T. Jarlborg, Comput. Mater. Sci. **28**, 287 (2003).

[34] R. Moore and Z.-X. Shen (private communication).